-RESEARCH PAPER-

International Journal of Mining and Geo-Engineering

IJMGE

IJMGE 58-4 (2024) 423-429

DOI: 10.22059/IJMGE.2024.381006.595189

Subsurface Characterization in Southeastern Asaluyeh Using DC Resistivity and Ground Penetrating Radar

Mohammadreza Najaftomraei [a,*], Sadegh Moghadam [b], Ramin Varfinezhad [b], Alireza Goudarzi [c] and Ali Faghih [a]

[a] *Ostim Technical University, Ankara, Turkey.*

[b] *Institute of Geophysics, Tehran university, Tehran, Iran.*

[c] *Graduate University of Advanced Technology, Kerman, Iran.*

[d] *Department of earth science, Shiraz University, Shiraz, Iran.*

Article History:

Received: 17 August 2024.

Revised: 16 October 2024.

Accepted: 29 October 2024.

ABSTRACT

This paper integrates the results of resistivity tomography and Ground Penetrating Radar (GPR) surveys to investigate the structural features of the southestern Asaluyeh site. By combining these geophysical methods with field observations, the study aims to provide a precise interpretation of subsurface conditions, focusing on identifying layer thicknesses, fractures, and weakened zones. The study utilized Direct Current (DC) resistivity and electromagnetic methods, i.e., GPR, both known for their high resolution, rapid data acquisition, and cost-effectiveness. Four DC resistivity and GPR profiles were analyzed where the results show three critical zones of varying layering in the resistivity sections. These zones include the gypsum layer in the marl host and fractures within the marl layer, with depths of influence ranging from 5 to 12 m. The GPR surveys, identified anomalies based on dielectric permittivity differences. The Joint interpretation of DC resistivity and GPR results revealed significant correlations between two methods, enhancing the understanding of subsurface features. Critical zones identified by both methods showed substantial overlap, confirming the presence of subsurface anomalies and providing a comprehensive view of the site's geological conditions. This integrated approach demonstrates the effectiveness of combining DC resistivity and GPR in subsurface investigations, offering valuable insights for similar geotechnical studies.

Keywords: *Ground Penetrating Radar (GPR), Southeastern Asaluyeh, Subsurface Anomalies, Integrated geophysical survey.*

1. Introduction

Geophysical methods have become increasingly utilized due to their lower cost and shorter time requirements compared to conventional geological methods, such as drilling and prospecting of ore deposits. Another feature of geophysical methods is their continuous interpretation. In drilling and prospecting, data belong to specific points, and extrapolating these data to other sections may not be accurate and may pose interpretation challenges.

Fractures can serve as pathways or barriers for fluid movement within the subsurface. In hydrogeology, the presence of fractures can enhance the permeability of low-permeability rocks, thus influencing groundwater flow and storage. This is particularly important in karst environments and fractured aquifers where groundwater resources are heavily dependent on the connectivity of fractures [1]. Accurate detection and characterization of near-surface fractures are essential for understanding subsurface processes and mitigating associated hazards. Over the past decades, considerable efforts have been devoted to developing and refining geophysical methods for this purpose, leading to significant advancements in fracture detection and characterization.

Different geophysical techniques exist for investigating geotechnical surveys, including seismic reflection and seismic refraction, electromagnetic methods, DC resistivity, and Ground Penetrating Radar (GPR) among which DC resistivity and GPR methods stand out in geotechnical studies. Early studies focused on the application of seismic reflection surveys for imaging near-surface fractures, utilizing differences in seismic wave velocities associated with fractured versus intact rock formations ([2], [3]). These pioneering efforts laid the foundation for subsequent research in fracture detection using geophysical approaches. However, seismic reflection surveys are limited by their sensitivity to shallow structures and their inability to accurately resolve fracture orientations and properties. Maunde and Bassey [4] identified fracture zones in Karshi through seismic refraction. Sheehan et al [5] enhanced the comprehension of the conditions under which seismic refraction methods are effective and examined the applicability of model results to actual field conditions. Research conducted by Jingjing et al [6] provides another example of detecting fracture zones using seismic refraction.

Electrical resistivity-based methods (e.g., DC resistivity, Very Low Frequency (VLF)) are among the most commonly used geophysical exploration techniques, which, besides their application in engineering studies, demonstrate significant efficiency in identifying and investigating various geological features, such as fractures and water-saturated fractured zones [7]. The study of these geological features is carried out by examining changes in the apparent resistivity. Researchers used electrical resistivity tomography (ERT) for mapping

* Corresponding author. *E-mail address:* najaftomraei@ostimteknik.edu.tr (M. Najaftomraei).

near-surface fractures ([8], [9], [10], [11], [12]). Two case studies were conducted by Ha et al. [13] to assess the suitability of electrical resistivity techniques for geotechnical and environmental challenges. Greve et al. [14] measured electrical anisotropy in a sand-filled lysimeter containing a plastic sheet to simulate an electrically insulating crack. Elis et al. [15] improved the understanding of the electrical response in 2D surveys for fracture zones mapping in crystalline rocks. Despite its success, ERT has inherent limitations, including the inability to differentiate between conductive fractures and saturated zones. Some studies have applied electromagnetic approaches in the detection of fractures. For instance, Li et al. [16] developed a rock burst model for coal and studied the relationship between energy accumulation and dissipation during the dynamic deformation and rupture of coal rock.

GPR emerged as another promising tool for fracture detection in the near surface. GPR utilizes high-frequency electromagnetic waves to image subsurface features, including fractures, with high resolution ([17]). Its non-invasive nature and ability to provide real-time, high-resolution images have made GPR a preferred choice for shallow fracture mapping in diverse geological settings.

It should be noted that each of the various geophysical methods has its own strengths and weaknesses. Therefore, the interpretation results of data obtained using only one geophysical approach may not be highly reliable in some cases. In these situations, combining two or more geophysical data sets can lead to a more accurate interpretation with higher credibility [18]. In recent years, significant advancements have been made in the integration of multiple geophysical methods for fracture characterization. Fehdi et al. [19] detected underground cavities near the Cherea area (NE Algeria) based on the sequential application of GPR and ERT. Mendieta [20] conducted multi-azimuthal 2D ERT and seismic refraction surveys in the Dry Creek Experimental Watershed to investigate deep fractures and anisotropy. Bahammou et al. [21] used resistivity profiling and VLF electromagnetic methods to detect fracture zones in the Zaouia Jdida, within the Errachidia basin. Hasan et al. [22] have carried out 2D ERT and self-potential (SP) in combination with the joint profile method (JPM) and boreholes to delineate the subsurface geological units. Carollo et al. [23] integrated seismic refraction tomography (SRT) and ERT to improve data interpretation accuracy, using both synthetic and real data. Gaballah et al. [24] used an integrated survey, including GPR and ERT, for mapping and evaluating a complex subsurface fracture network in Eocene limestone at the Al-Mokattam site, Egypt.

In this study, efforts have been made to integrate the results of ERT and GPR surveys to investigate the structure features of the southeastern Asaluyeh. The combined results of these studies, along with field observations, aim to provide a more precise interpretation of subsurface conditions in the study area. Furthermore, subsurface features, such as fractures, and weakened zones were selected as suitable targets for identification using both resistivity and GPR approaches.

2. Methodology

In the present study, both direct current (DC) resistivity and electromagnetic methods, particularly GPR, have been utilized for investigating the subsurface characteristics of geological layers. These methods possess high-resolution capabilities, enable rapid data acquisition, and are cost-effective. Additionally, advanced modelling and inversion techniques are available in this field, facilitating more accurate interpretations, especially in geologically complex areas [25]. From an electrical perspective, anomalies characterized by low electrical resistivity may be attributed to high salinity content in pore fluids, the presence of clay, particle size distribution, or a combination thereof [26]. Consequently, areas prone to fracturing can be identified using electrical resistivity methods prior to ground subsidence [27]. The rationale behind employing the geoelectrical method lies in its superior resolving power for identifying water-bearing layers within fracture zones, a critical factor in expediting groundwater flow [28]. However, the use of GPR is preferred due to its high accuracy in calculating layer thicknesses and shallow-depth fracturing, particularly in determining common fractured zones.

2.1. GPR approach

GPR is a non-destructive geophysical method known for its high-resolution capabilities. It involves the transmission of high-frequency electromagnetic waves into the ground and recording the reflected waves from subsurface interfaces, thereby facilitating subsurface investigation at shallow depths. This technique employs electromagnetic (EM) waves to visualize subsurface structures in geological, archaeological, and other environmental applications [29]. The detailed interpretation of GPR features is primarily dependent on temporal resolution. Enhancing the temporal resolution of GPR data is crucial for accurately characterizing underground structures [30]. The benefits of sparse signal processing using the majorization-minimization (MM) method for GPR signal compression were examined. This approach involves minimizing the cost function using L1 and L2 norms, and it considers the banded structures of matrices arising from the sparse deconvolution problem.

2.2. GPR processing and Attribute

GPR processing includes time-zero correction, Dewow, gain, background removal, and a non-local mean filter. We use time-zero correction to accurately position the starting point of traces on the surface and reflections in their true locations. Dewow is employed to eliminate the impact of low-frequency, unwanted reflections that overlap with high-frequency reflections in GPR sections. Gain is applied to offset the decrease in power of electromagnetic waves as they penetrate deeper. Background removal is utilized to eliminate direct aerial and ground waves. Finally, we applied the non-local filter to eliminate random noise in GPR sections [17].

Also, we extracted the instantaneous energy of a signal x(t) which may be monitored using the instantaneous energy operator, sometimes referred to as the instantaneous envelope (E). The operator is defined by taking the square of the values of its analytic form:

$$E(x(t)) = (x(t) + iH(x(t)))^2 \quad (1)$$

Where H is the Hilbert transform and i^2=-1. By the derivative function as the frequency-weighted filter, we were able to compute the instantaneous energy with more accuracy [31].

2.3. DC resistivity method

DC resistivity method has the appropriate capability to identify anomalies with small dimensions and areas with complex geology. To obtain apparent resistivity, direct or alternating electric current with a low frequency (generated by a battery or generator) is sent from two installed electrodes (A, B) on the ground surface into the ground. The voltage resulting from this current is measured inside the ground by two electrodes (M, N). The electrical conductivity of rocks generally depends on the mineral composition forming them. If a rock is highly compacted, it will have high electrical resistivity, but due to the defects and fractures present in rocks, their resistivity can vary significantly [32]. Therefore, the effective factors influencing electrical resistivity include I) the volume of defects and fractures in rocks, II) their distribution and interrelation, III) the volume of defects and fractures containing water, IV) the electrical conductivity ability of water present in rocks, and V) the mineral composition forming the rocks. In many geological conditions, two-dimensional surveys using DC resistivity can yield useful results that complement and supplement the results obtained by other geophysical methods. For example, GPR method provides acceptable images of subsurface layers, but its penetration depth depends on the type of subsurface layers and the used antenna frequency. Using lower-frequency antennas can increase the penetration depth of the ground-penetrating radar method; however, with increasing penetration depth, the resolution of obtained sections decreases. Therefore, two-dimensional DC resistivity method can be performed in conjunction with the GPR method, as these methods can provide complementary information about subsurface layers with

accuracy and acceptable quality [33]. Two-dimensional DC resistivity surveys are usually carried out using a large number of electrodes consisting of a multi-strand cable and an electronic switch box through which measurements are made by selecting four electrodes (two current electrodes and two potential electrodes). Figure 1 illustrates the typical setup for the Wenner-Schlumberger configuration. Typically, a constant value is considered as the electrode spacing distance, denoted by the quantity 'a' in the relevant equations. The most commonly used arrays in tomographic surveys include Wenner-Schlumberger and dipole-dipole arrays, where the first one is used in this study to achieve layering status and existing fractures in each profile.

The quantitative interpretation of DC resistivity data typically necessitates inverse modelling. An exception is the continuous wavelet transform (CWT) technique introduced by Barbolla et al. [34] for interpreting DC resistivity data, as no other alternative approaches exist for the quantitative interpretation of the DC resistivity method.

For addressing the DC resistivity problem, Loke et al. [35] described a versatile algorithm implemented in the widely used RES2DINV® software. This software employs two optimization iterative approaches that can be selected alternatively. The first approach is the L2 norm smoothness-constrained optimization method, which produces a model with smooth resistivity variations. This method minimizes the objective function at each kth iteration:

$$\psi(m_k) = g_k^T g_k + \mu_k m_k^T W_m m_k \quad (2)$$

In this expression, μ_k is the regularization parameter, $m_k$is the model vector, and $g_k = d - F(m_k)$ is the data-misfit vector between the logarithm of the apparent resistivity from measurements and that calculated from the model m_k. Using the gradient of the objective function, the Gauss-Newton method of least squares is applied to solve the following system of equations [36].

$$(J_k^T J_k + \mu_k W_m) \Delta m_k = J_k^T g_k - \mu_k W_m m_{(k-1)} \quad (3)$$

where is J_k the Jacobian matrix. Once the model variation Δm_k is estimated, the model is updated as $m_k = m_{k-1} + \Delta m_k$.

The second method is a L1-norm based optimization method, based on the iteratively reweighted least-squares algorithm[37]:

$$(J_k^T J_k + \mu_k W_m) \Delta m_k = J_k^T R_d g_k - \mu_k W_m m_{(k-1)} \quad (4)$$

where R_d is a re-weighting matrix. We used L2 norm for the inversion of the measured DC resistivity data.

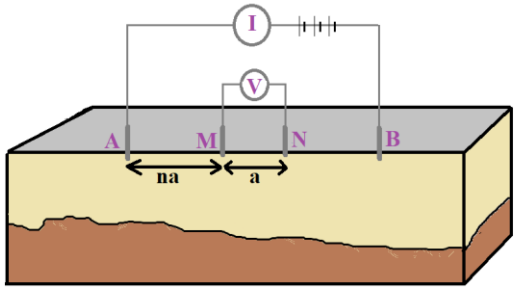

Fig1. Schematic diagram of the DC resistivity using the Wenner-Schlumberger array.

3. Study area

The southeast of Asaluyeh in the Koushknar region, part of the Parsian County in Hormozgan Province, is an area with diverse and complex geology. This region, due to its location in the Zagros fold belt and its proximity to the Persian Gulf, possesses unique geological features. The Zagros region, especially in the southeastern parts of Asaluyeh, has complex structures formed due to tectonic activities over millions of years. This area is part of the Zagros fold and thrust belt, resulting from the collision of the Arabian and Iranian tectonic plates. The rock units and formations in this area include a) Cretaceous Formations: These formations include shales, limestones, and sandstones deposited during the Cretaceous period. These formations often contain marine fossils, indicating a marine environment at that time. b) Cenozoic Formations: These formations consist of thick sequences of limestone, marl, and gypsum, primarily formed during the Tertiary period (Paleogene and Neogene). c) Quaternary Formations: These formations include alluvial and fluvial deposits formed in the recent geological periods. These sediments often consist of sand, gravel, and silt. In terms of tectonic activities, the Zagros region, due to the tectonic pressures from the collision of the Arabian and Iranian plates, has numerous folded structures and faults. These tectonic activities have resulted in the formation of hills, mountains, and deep valleys. This area, due to its complex geological structures, has numerous natural resources, including oil and gas reserves. The South Pars gas field, one of the largest gas fields in the world, is located in this region. Industrial activities and the extraction of natural resources in this area can have serious environmental impacts. Balancing industrial development with environmental protection is one of the main challenges in this region.

The study area is situated on the southern edge of the Madar Anticline in the Zagros Mountains, southwestern Iran. This anticline, an asymmetric fault-related fold striking NW-SE, spans between the Bushehr and Hormozgan provinces along the Persian Gulf coast. The southern edge of the anticline exhibits a steeper dip compared to the northern edge, with a maximum dip of 35 degrees. The primary rock outcrops in the anticline are the Aghajari Formation (comprising marlstone, gypsum, and sandstone) and the Bakhtiari Formation (conglomerate). While the northwestern parts of the anticline are predominantly covered by the Bakhtiari Formation, the site of interest exposes only the Aghajari Formation. Excavation and leveling activities for a construction project on the southern edge of the anticline have resulted in the formation of significant and large cracks in the study area. To better understand the causes of these cracks and assess the risk of further expansion, DC resistivity measurement and GPR survey were conducted. Figure 2 provides a general view of the study area provided by Google Earth map, including four interested profiles. The green line in Figure 2 corresponds to the geological cross-section shown in Figure 3. The geological section of subsurface is displayed in Figure 3 where inclined gypsum is generally immersed in an Aghajari formation, which is mainly compose of Marne.

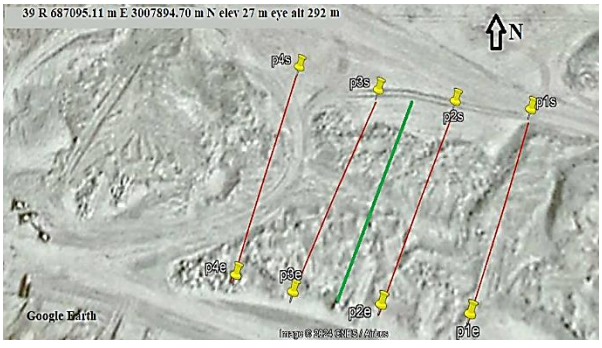

Fig. 2. A general view of the study area and development of several large NW-SE oriented cracks on the southern limb of the Madar Anticline.

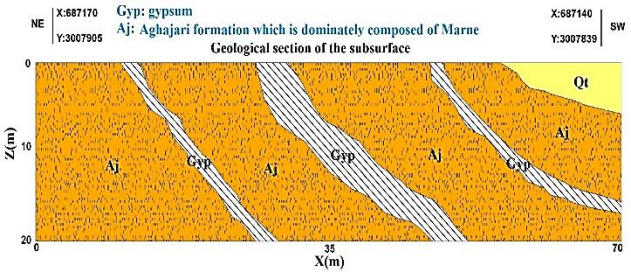

Fig. 3. Geological section of the subsurface.

3.1. Data measurements

In this study, an attempt was made to integrate the results obtained from the DC resistivity tomography method and GPR to examine the critical areas detected by each of these methods for a more precise and reliable interpretation. Although the tomography method provides reliable results in areas with complex geology, the GPR method was also utilized. GPR data were collected from an area where shortly before the survey, major cracks appearedat at the surface. The survey was carried out using a MALA GPR shielded antenna with an 80 MHz antenna.GPR profiles were collected in the field using RAMAC Groundvision GPR measurement software to make 2D images. At first, four DC resistivity were measured using the Wenner-Schlumberger array with an electrode spacing of 4 m. All profiles used in this study have lengths of 76m, including 20 electrodes which are directed from north-east to south-west. For conducting geoelectric studies, the utilized equipment and tools were the ABEM-SAS-1000 geoelectric device, brass and steel electrodes, a Global Positioning System (GPS) for coordinate system localization, grounding rods, cables, and connecting wires. Considering the project's sensitivities and the exceptional importance of the existing blocks in the area, two-dimensional tomographic profiles with high-resolution capabilities for subsurface layers to a depth of approximately 16 meters have been acquired. Then, four profiles of GPR survey are alonge the same profile, as Dc resistivity profiles which are presented in the following sections. Since geophysical methods, including GPR are based on the physical properties of materials (dielectric permittivity), and the detection is based on the difference between the physical parameters of the target and the environment, changes based on these parameters are taken into account and are recognized and examined as anomalies.

3.2. Joint interpretation of DC resistivity and Ground Penetrating Radar (GPR)

In order to make the interpretation of the measured data sets, the joint interpretation of DC resistivity data inversion and processed GPR data is applied. Measured apparent resistivity data and GPR data for the profile 1 are displayed in Figure 4 where a reliable interpretation may not be made from these measured data. However, for this special case and for DC resistvity, two resistive anomalies can be qualitatively interpreted for x coordinates from 40 to 60 m. Therefore, inversion (for DC resistivity), processing, and attributes (for GPR) are required in order to detect subsuface anomalies which are demonstrated in Figure 5. For all resistivity inverse sections, three critical zones with varying layering were observed, and in all four profiles, the first zone is related to the gypsum layer surrounded by Marne, which affects depth of less than 5 meters in the resistivity sections. Beyond this depth, due to the absence of subsurface resistivity changes, there are no geophysical changes in the subsurface layers. Horizontal extension of the first critical zone is approximately 10 meters.

The second critical zone is related to the fracture in the Marne layer along with the gypsum layer immersed in marl, which has an effective depth of approximately 10 meters for profiles 1-3 and 12 meters for profile 4 in the resistivity section. Considering the gypsum layer's resistivity and the absence of changes in layering direction, it is expected that the extent of fracturing to depths of about 10 m may increase due to gypsum layer dissolution. Beyond the depth of 10 meters (for profiles 1-3) and 12 meters (for the profile 4), due to the absence of subsurface resistivity changes, there are no geophysical changes in the subsurface layers. The horizontal extension of this critical zone is 16 m for P1, P2 and P3, and 13 m for P4.

The third critical zone corresponds to the gypsum layer encompassed by the Marne, so that the gypsum layer's depth of effect is less than 5 m. Beyond this depth, due to the absence of subsurface resistivity changes, there are no geophysical changes in the subsurface layers. The horizontal length of this critical zone is 8 m for P1and P2, while it is 7 m for P3 and P4.

For the GPR approach, processed sections of measured data and the Instantaneous Energy Attribute (IEA) are presented. From the processed data sections, the second critical zone was clearly detected, the third critical zone was relatively noticeable, especially for profiles 1 and 2, but the first critical zone was not discerned except in profile 1. Sections derived from the implementation of IEA clearly demonstrate the recovery of the second critical zone, while the third critical zone may be discerned in sections of profiles 1, 2 and 3 (for profile 4, it is difficult to conclude the presence of the third critical zone). It should be mentioned regarding the first critical zone that a weak anomaly may be distinguished (at x=25 m) for profiles 1, 2 and 3; however, this weak anomaly may not be detected in the section 4. On aggregate, it can be concluded that this the utilized IEA helped use detect more anomalies with greater resolution than the processed GPR data. Indeed, IEA sections show more consistency with DC resistivity inversion results about subsurface targets.

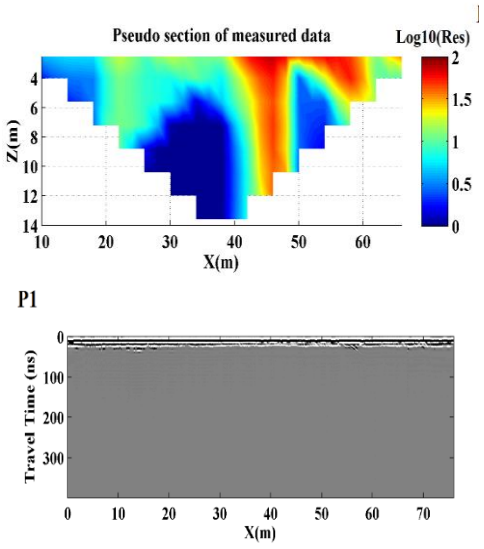

Figure 4. Measured apparent resistivities (Up) and GPR (Down) data sets.

Since GPR is a high-resolution method, we may expect that GPR would detect anomalies better than DC resistivity, but according to the obtained results, DC resistivity approach shows critical zones better than GPR. This issue may be hidden in the contrasts of resistivities and dielectric constants between anomalies and background medium. Indeed, resistivity contrast is likely more significant than dielectric contrast.

Now two important questions should be addressed regarding DC resistivity and GPR results: I) Why is the second critical zone clearly detected in all sections using both approaches? II) Why is the recovery of critical zones not achieved at greater depths for all anomalies and by both methods in spite of continuations of these zones to depths greater than 15 m (considering the geological section shown in Figure 3)?

The second anomaly is considerably thicker than the first and the third ones, so its effect is more significant on the measured data at the surface (see resistivity pseudo-section in Figure 4 and the processed GPR data in Figure 5). Hence, the detection of this critical zone is much easier than the other ones. At greater depths, we are confronted with two issues: 1) increasing the depth of exploration is achieved by increasing the electrode separation for DC resistivity and increasing time intervals for GPR waves, so it is reasonable to have lower resolution at greater depths for both methods. 2) Furthermore, DC resistivity measurements are collected using the Wenner-Schlumberger array which does not provide enough data coverage on the left and right parts of the area at greater depths; thus, recovery problem about the first and the second anomalies is intensified. The results of processing, modelling, and interpreting the collected data indicated that the integration of these two methods is highly effective in identifying phenomena, such as existing fractures. Based on this case study, we noticed that DC

resistivity and GPR show relatively good correspondence in detecting critical zones, but complete consistency cannot be expected, because they are searching for subsurface sources using different paramters (resistivity and dielectric constant). The joint interpretation of DC resistivity and GPR results across all profiles indicates a promising correlation between two methods in identifying critical zones. Overlapping detected zones suggest that both methods are sensitive to similar subsurface anomalies, potentially indicating changes in lithology, moisture content, or other geophysical properties. This complementary use of both methods enhances the reliability and detail of subsurface investigations, providing a robust framework for identifying and characterizing critical zones.

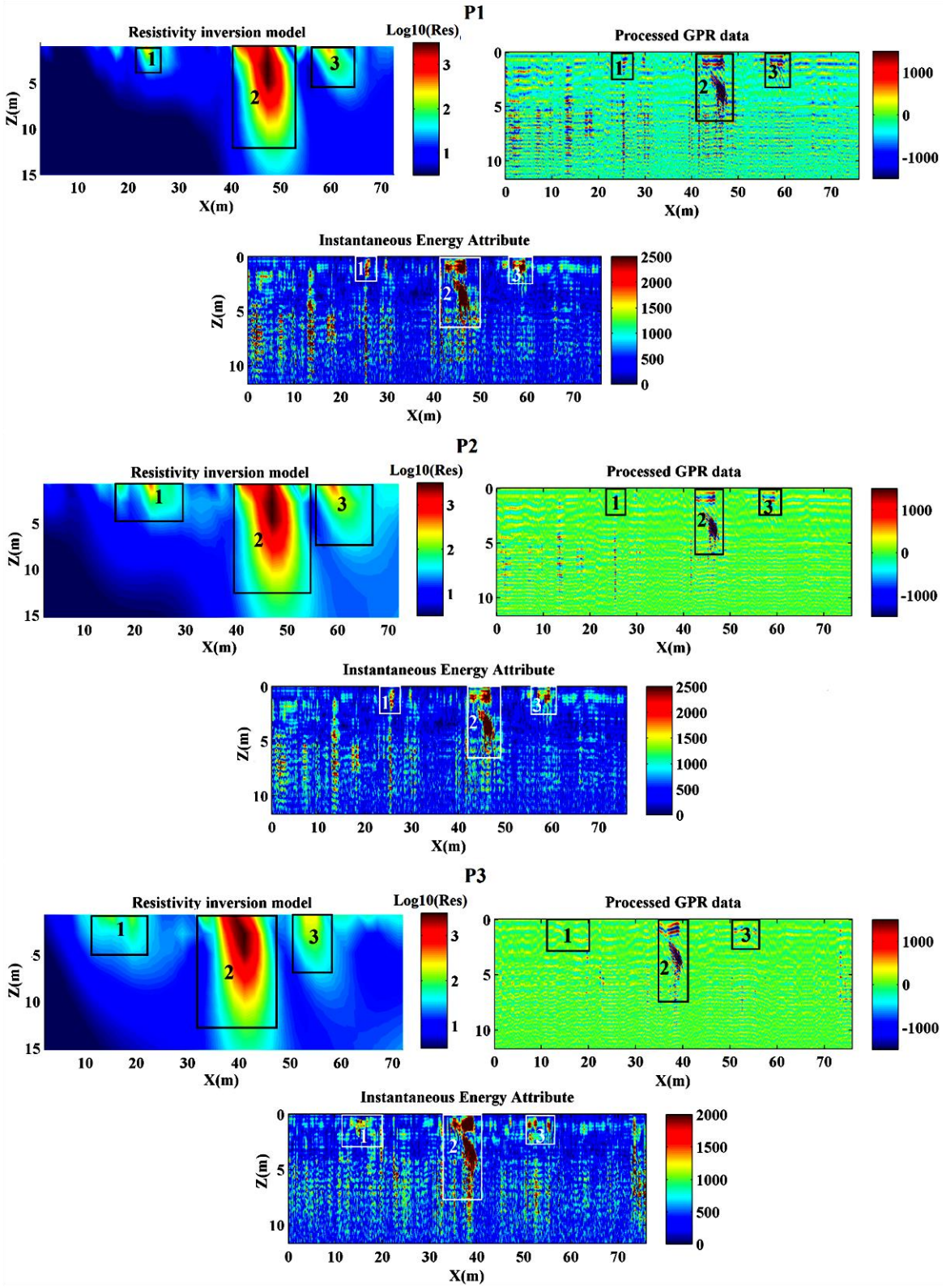

Figure 5. Inverted resistivity models (left), the processed GPR sections (right) and IEA sections (bottom) for all the profiles.

4. Conclusion

This study successfully integrates resistivity tomography and Ground Penetrating Radar (GPR) surveys to investigate the tectonic features in the southestern Asaluyeh. By combining these geophysical methods with field observations, we have achieved a more precise interpretation of subsurface conditions, particularly in identifying layer thicknesses, fractures, and weakened zones. The results demonstrate a high degree of agreement and compatibility between DC resistivity and GPR in delineating lithological features, highlighting the effectiveness of using both methods together. Our investigation utilized high-resolution DC resistivity and GPR methods, which enabled rapid data acquisition and were cost-effective. Advanced modelling and inversion techniques further enhanced the accuracy of our interpretations, especially in this geologically complex area. Four tomographic profiles were analyzed, revealing three critical zones with varying layering and specific features within the gypsum and marl layers. The resistivity data provided valuable depth profiles, while the GPR data identified anomalies based on dielectric permittivity differences. The joint interpretation of the DC resistivity and GPR results showed significant correlations, enhancing our understanding of subsurface conditions. Critical zones identified by both methods exhibited substantial overlap, confirming the presence of significant subsurface anomalies. This integrated approach allowed for a comprehensive analysis, revealing multiple distinct features and providing a clear view of the site's geological conditions. The findings of this study underscore the benefits of integrating resistivity tomography and GPR surveys for subsurface investigations. The combined use of these methods offers enhanced resolution and accuracy, making it a valuable approach for geotechnical studies in similar settings. Future research could expand on this approach, applying it to other areas with complex geological conditions to further validate its efficacy and explore additional applications.

Acknowledgment

The authors would like to express their gratitude to everyone who contributed to the successful completion of this study. Special thanks to the field and technical teams for their support in conducting the resistivity tomography and Ground Penetrating Radar (GPR) surveys. We also appreciate the valuable input from our colleagues (especially Dear Mani Vakili) and reviewers, which significantly improved the quality of this work. It is important to note that the data used in this study is not available due to the nature of the project and the constraints related to data sharing policies.

References

[1] Cook, P. G., Favreau, G., Dighton, J. C., & Tickell, S. (2006). Hydrology of a fractured rock aquifer under rainfall and irrigation recharge, Clare Valley, South Australia. Hydrogeology Journal, 14(7), 1201-1214. https://doi.org/10.1007/s10040-006-0034-6

[2] Schmelzbach, C., Horstmeyer, H., & Juhlin, C. (2007). Shallow 3D seismic-reflection imaging of fracture zones in Crystalline Rock. GEOPHYSICS, 72(6). https://doi.org/10.1190/1.2787336

[3] Sicking, C., & Malin, P. (2019). Fracture seismic: Mapping subsurface connectivity. Geosciences, 9(12), 508. https://doi.org/10.3390/geosciences9120508

[4] Maunde, A., & Bassey, N. E. (2017). Seismic refraction investigation of fracture zones and bedrock configuration for geohydrologic and geotechnical studies in part of Nigeria's Capital City, Abuja. Journal of Earth Sciences and Geotechnical Engineering, 7(2), 91-102.

[5] Sheehan, J. R., Doll, W. E., Watson, D. B., & Mandell, W. A. (2005). Application of seismic refraction tomography to karst cavities. US geological survey karst interest group proceedings, Rapid City, South Dakota, 29-38.

[6] QIN JingJing, LIU BaoJin, XU HanGang, SHI JinHu, TAN YaLi, HE YinJuan, GUO XinJing. 2020. Exploration of shallow structural characteristics in the Suqian segment of the TanLu fault zone based on seismic refraction and reflection method. Chinese Journal of Geophysics (in Chinese), 63(2): 505-516, doi: 10.6038/cjg2020N0144

[7] Varfinezhad, R., Oskooi, B., & Fedi, M. (2020). Joint inversion of DC resistivity and magnetic data, constrained by cross gradients, compactness and depth weighting. Pure and Applied Geophysics, 177(9), 4325–4343. https://doi.org/10.1007/s00024-020-02457-5

[8] Carrière, S. D., Chalikakis, K., Sénéchal, G., Danquigny, C., & Emblanch, C. (2013). Combining Electrical Resistivity Tomography and Ground Penetrating Radar to study geological structuring of karst Unsaturated Zone. Journal of Applied Geophysics, 94, 31–41. https://doi.org/10.1016/j.jappgeo.2013.03.014

[9] Li, S., Liu, B., Nie, L., Liu, Z., Tian, M., Wang, S., ... & Guo, Q. (2015). Detecting and monitoring of water inrush in tunnels and coal mines using direct current resistivity method: a review. Journal of Rock Mechanics and Geotechnical Engineering, 7(4), 469-478.

[10] Szalai, S., Kovács, A., Kuslits, L., Facskó, G., Gribovszki, K., Kalmár, J., & Szarka, L. (2018). Characterisation of fractures and fracture zones in a carbonate aquifer using electrical resistivity tomography and pricking probe methodes. Journal of Geoscience and Environment Protection, 06(04), 1–21. https://doi.org/10.4236/gep.2018.64001

[11] Yanis, M., Ismail, N., & Abdullah, F. (2021). Shallow structure fault and fracture mapping in Jaboi Volcano, Indonesia, using VLF–EM and electrical resistivity methods. Natural Resources Research, 31(1), 335–352. https://doi.org/10.1007/s11053-021-09966-7

[12] Parnow, S., Oskooi, B., & Florio, G. (2021). Improved linear inversion of low induction number electromagnetic data. Geophysical Journal International, 224(3), 1505-1522.

[13] Ha, H. S., Kim, D. S., & Park, I. J. (2010). Application of electrical resistivity techniques to detect weak and fracture zones during underground construction. Environmental Earth Sciences, 60, 723-731.

[14] Greve, A. K., Acworth, R. I., & Kelly, B. F. (2010). Detection of subsurface soil cracks by vertical anisotropy profiles of apparent electrical resistivity. Geophysics, 75(4), WA85-WA93.

[15] Elis, V. R., Bondioli, A., Ustra, A. T., Carlos, I. M., & Pozzo, H. Â. P. D. (2019). Resistivity imaging for identification of fracture zones in crystalline bedrock in Brazil. Sustainable Water Resources Management, 5, 1089-1101.

[16] Li, X., Chen, S., Wang, E., & Li, Z. (2021). Rockburst mechanism in coal rock with structural surface and the microseismic (MS) and electromagnetic radiation (EMR) response. Engineering Failure Analysis, 124, 105396.

[17] Oskooi, B., Parnow, S., Smirnov, M., Varfinezhad, R., & Yari, M. (2018). Attenuation of random noise in GPR data by image processing. Arabian Journal of Geosciences, 11, 1-10.

[18] Afshar, A., Abedi, M., Norouzi, G., & Riahi, M. (2015). Geophysical investigation of underground water content zones using electrical resistivity tomography and ground penetrating radar: A case study in Hesarak-Karaj, Iran. Engineering Geology,

196, 183–193. https://doi.org/10.1016/j.enggeo.2015.07.022

[19] Fehdi, C., Nouioua, I., Belfar, D., Djabri, L., & Salameh, E. (2014). Detection of underground cavities by combining electrical resistivity imaging and ground penetrating radar surveys: A case study from Draa Douamis area (North East of Algeria). H2Karst research in limestone hydrogeology, 69-82.

[20] Mendieta, A. (2017). Seismic Refraction and Electrical Resistivity Tests for Fracture Induced Anisotropy in a Mountain Watershed.

[21] Bahammou, Y. A., Benamara, A., Ammar, A., & Dakir, I. (2019). Fracture zones detection for groundwater exploration integrating Resistivity Profiling and Very Low Frequency electromagnetic methods (Errachidia basin, Morocco). Contributions to Geophysics and Geodesy, 49(2), 181-194.

[22] Hasan, M., Shang, Y. J., Jin, W. J., & Akhter, G. (2019). Investigation of fractured rock aquifer in South China using electrical resistivity tomography and self-potential methods. Journal of Mountain Science, 16(4), 850-869.

[23] Carollo, A., Capizzi, P., & Martorana, R. (2020). Joint interpretation of seismic refraction tomography and electrical resistivity tomography by cluster analysis to detect buried cavities. Journal of Applied Geophysics, 178, 104069.

[24] Gaballah, M., & Alharbi, T. (2022). 3-D GPR visualization technique integrated with electric resistivity tomography for characterizing near-surface fractures and cavities in limestone. Journal of Taibah university for science, 16(1), 224-239.

[25] Telford, W. M., Geldart, L. P., & Sheriff, R. E. (1990). Applied Geophysics. Cambridge University Press.

[26] Palacky, G. J. (1988). Resistivity characteristics of geological targets. In M. N. Nabighian (Ed.), Electromagnetic Methods in Applied Geophysics: Volume 1, Theory (pp. 53-129). Society of Exploration Geophysicists.

[27] Dahlin, T. (2001). The development of DC resistivity imaging techniques. Computers & Geosciences, 27(9), 1019-1029.

[28] Loke, M. H., Chambers, J. E., Rucker, D. F., Kuras, O., & Wilkinson, P. B. (2013). Recent developments in the direct-current geoelectrical imaging method. Journal of Applied Geophysics, 95, 135-156.

[29] Bednarczyk, Z., & Szynkiewicz, A. (2015). Applied engineering geology methods for exemplar infrastructure projects in Malopolskie and Podkarpackie provinces. In Engineering Geology for Society and Territory-Volume 6: Applied Geology for Major Engineering Projects (pp. 203-210). Springer International Publishing.

[30] Moghaddam, S., Oskooi, B., Goudarzi, A., & Azadi, A. (2019). The comparative sense of sparse deconvolution and least-squares deconvolution methods in increasing the temporal resolution of GPR data. Arabian Journal of Geosciences, 12, 1-10.

[31] Zhang, X., Hu, X., Qiu, Z., Feng, X., & Qin, Y. (2023). Extraction of the GPR instantaneous centroid frequency based on the envelope derivative operator and ICEEMDAN. Remote Sensing Letters, 14(5), 469-478.

[32] Koefoed, O. (1979). Geosounding Principles 1: Resistivity Sounding Measurements. Elsevier.

[33] Hubbard, S. S., & Rubin, Y. (2000). Hydrogeological parameter estimation using GPR and DC resistivity measurements. Journal of Environmental and Engineering Geophysics, 5(2), 45-58

[34] Barbolla, D. F., Negri, S., & Fedi, M. (2022). Analysis of direct current resistivity data using continuous wavelet transform. GEOPHYSICS, 87(5). https://doi.org/10.1190/geo2021-0111.1

[35] Loke, M.H., Acworth, R., Dahlin, T., 2003. A comparison of smooth and blocky inversion methods in 2D electrical imaging surveys, Exploration Geophysics, 34(1), 182-87.

[36] Loke, M. H., & Dahlin, T. (2002). A comparison of the Gauss–Newton and quasi-Newton methods in resistivity imaging inversion. Journal of Applied Geophysics, 49(3), 149–162.

[37] Wolke, R., & Schwetlick, H. (1988). Iteratively reweighted least squares: algorithms, convergence analysis, and numerical comparisons. SIAM journal on scientific and statistical computing, 9(5), 907-921.